AIAA AVIATION Forum
5-9 June 2017, Denver, Colorado
35th AIAA Applied Aerodynamics Conference

10.2514/6.2017-3917

Acoustic Prediction of High Speed Propeller Noise Using URANS and a Ffowcs Williams-Hawkings Solver

Jason R. Hambrey[1] and Daniel Feszty[2]
Carleton University, Ottawa, ON, K1S 5B6, Canada

Sid-Ali Meslioui[33]
Pratt & Whitney Canada, Longueuil, QC, J4G 1A1, Canada

and

Jong Park[4]
Pratt & Whitney Canada, Longueuil, QC, J4G 1A1, Canada

The prediction of propeller noise has become increasingly important as aircraft noise standards continue to require quieter design of turboprop aircraft. However, aeroacoustic simulations have historically used relatively simple flow models to describe the flow field of a propeller as part of an aeroacoustic simulation. In particular, the capability of an unsteady Reynolds-Averaged Navier-Stokes simulation has not been tested. An unsteady Reynolds-Averaged Navier-Stokes simulation, combined with the Ffowcs Williams-Hawkings Solver, is used to simulate the noise generated by a high speed 8-bladed propeller. Simulations were conducted using the STAR CCM+ code, using a verified 7.6 million cell mesh. This resulted in good prediction of propeller harmonics relative to experimental values.

Nomenclature

C_P	=	power coefficient
D	=	propeller diamter
p	=	pressure
p'_T	=	thickness noise
p'_L	=	loading noise
p_0	=	far field pressure
P	=	propeller power
$\boldsymbol{P}_{ij}$	=	compressive stress tensor
ρ	=	density
ρ_0	=	far field density
$\boldsymbol{r}$	=	distance from propeller surface to microphone
$d\tilde{\boldsymbol{a}}$	=	differential surface area
f	=	function describing the Ffowcs Williams-Hawkings surface
$\boldsymbol{v}_i$	=	surface velocity in the x_i direction
$\boldsymbol{v}_n$	=	surface velocity component normal to the surface
$\boldsymbol{u}_i$	=	fluid velocity in the x_i direction
$\boldsymbol{u}_n$	=	fluid velocity component normal to the surface
$\boldsymbol{n}$	=	surface normal vector
δ_{ij}	=	Dirac delta function
ω	=	rotational speed

[1] Research Associate, Department of Mechanical and Aerospace Engineering, Carleton University.
[2] Associate Professor, Department of Mechanical and Aerospace Engineering, Member of AIAA.
[3] Manager & Technical Fellow, Acoustics
[4] Senior Engineer, Acoustics

I. Introduction

PROPELLERS are of particular interest to the aerospace industry because of their efficient operation, operating at high efficiency until flight speeds of about 0.65 Mach[1], with advanced propeller design enabling efficient operation up to cruise speeds of 0.8 Mach[2]. At these speeds the efficiency of propellers can be significantly higher than that of turbofans or turbojets and consequently their utilization is of continued interest for subsonic aircraft in a competitive industry with increasing fuel costs.

Although they are popular for short-haul flights, an impediment to the use of turboprop engines is the noise generated by the propeller. Quiet operation is desired in order to ensure passenger comfort in the cabin as well as to conform to increasingly strict international noise standards. The International Civil Aviation Organization (ICAO) sets international standard noise level requirements for aircraft manufacturers, with noise measurement points set at the approach before landing and the takeoff point for turboprops. The ICAO standards have become increasingly stringent regarding aircraft noise limits for certification, with ICAO Annex 16 establishing Chapter 14 to come into effect for new aircraft beginning in 2017. Chapter 14 requires a reduction of 7 dB or greater in effective perceived noise (EPNdB) from Chapter 4, which is currently in effect. As a result, noise reduction for aircraft is particularly important and understanding the prediction tools and utilizing them to predict noise in new designs is essential.

Propeller noise models have been developed as early as 1919, though, at the time, they were quite limited due to a lack of computational power and experimental equipment[3,4]. In 1936, Gutin[5] was the first to develop a noise prediction theory which correctly described the noise generation process in propellers. Significant progress was then made between the 1950s and the 1970s as a result of the advent of computers and the acoustic analogy first proposed by Lighthill[6]. This work led to the derivation of the Ffowcs Williams and Hawkings (FW-H) Equations in 1969[7], upon which most of the propeller noise models are currently based[4]. All these models share the concept that blade loads and fluid displacement around the propeller are predicted via some sort of aerodynamic method in the rotating frame and then converted to an acoustic signal in the non-rotating frame. The blade loadings are either represented as a spanwise distribution along the quarter-chord line (Gutin) or as a surface pressure distribution (FW-H).

Many computational studies have been performed to validate different noise models on various experiments, however, relatively few couple an aerodynamic and an aeroacoustic prediction. A list of such studies available in the literature is presented in Table 1.

Table 1. Aerodynamic and Aeroacoustic Simulations of Propeller Noise Validated by Experiment

Author	Year	Aerodynamic Calculation	Acoustic Calculation
Succi et al.[8]	1982	Lifting Line	FW-H
Schulten[9]	1988	Blade Element Momentum Theory*	Kirchoff-Helmholtz
Nallasamy et al.[10]	1989	Euler Equation	FW-H
Whitefield et al.[11]	1989	Euler Equation	FW-H
Schulten[12]	1996	Lifting Line	Kirchoff-Helmholtz
Schulten[13]	1997	Lifting Line	Kirchoff-Helmholtz
De Gennaro et al.[14]	2010	Reynolds Averaged Navier-Stokes	FW-H
Boots and Feszty[15]	2016	Potential Flow and Free Vortex	FW-H

*coupled with a two dimensional method to predict propeller section aerodynamics

As can be seen from Table 1, the utilization of higher level CFD methods has not been explored as part of an acoustic prediction. There is only one published computational aeroacoustic study using a Reynolds-Averaged Navier-Stokes (RANS) simulation which can enable much more accurate and robust calculation of the aerodynamic forces and flow field than the other methods listed, though at higher computational cost. RANS methods generally are significantly more expensive compared to the other methods listed in Table 1, but enable higher fidelity

modeling of turbulent, viscous, and separation effects. Given the lack of studies utilizing RANS and the prevalence of simpler methods, it is of interest to investigate how accurately and feasibly RANS methods, coupled with an acoustic solver, can predict propeller noise

The previous study utilizing RANS by De Gennaro et al.[14], published in the European Conference on Compuational Fluid Dynamics, is based on the steady state simulation of a slice of the domain with periodic boundary conditions. This can be viewed as an entry level simulation for RANS, being the simplest and least expensive method to compute the aerodynamics of a rotating blade using RANS. However, De Genaro et al. does not provide comparison to unsteady RANS (URANS) results nor provide a comparison to a full rotating domain which models the entire propeller rather than a periodic blade. Additionally, only partial data from the microphones are described. This paper aims to present an aeroacoustic validation case from a URANS simulation utilizing a full domain.

III. Methodology

A. Selection of Validation Case

In selecting propeller validation cases, the focus was on the prediction of noise for propellers representative of those currently in production for turboprop aircraft, namely, straight-bladed propellers with subsonic tip speeds. The experiment selected was performed by James Dittmar in the NASA Lewis Research Center 8-by-6 foot wind tunnel in 1989, in a study of aerodynamic and aeroacoustic results of an SR-2 propeller [16]. This experiment is particularly valuable because of repeated, similar results from additional data collected in a different wind tunnel and in flight[17]. The experimental conditions which were simulated are summarized in Table 2. Acoustic measurements were made at 12 microphones located 0.3 propeller diameters from the propeller tip, shown, along with the propeller rig test setup in a wind tunnel as shown in Fig. 1.

Table 2. Experiment Conditions for SR-2 Test Case 2

Property	Value
Propeller	SR-2
Propeller diameter	0.622 m
Number of Blades	8
Blade Pitch Angle	59
Mach Number	0.6
RPM	6487

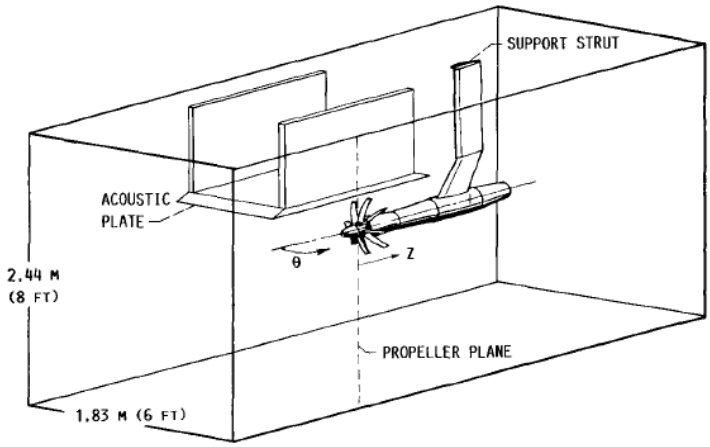

TRANSDUCER (PLATE 0.3 DIAMETER FROM TIP)											
1	2	3	4	5	6	7	8	9	10	11	12
TRANSDUCER DISTANCE FROM PROPELLER PLANE, Z, CM (IN.)											
-46.7 (-18.4)	-41.7 (-16.4)	-30.5 (-12.0)	-16.0 (-6.3)	-8.9 (-3.5)	0.8 (0.3)	8.9 (3.5)	12.4 (4.9)	18.0 (7.1)	25.0 (9.9)	28.7 (11.3)	42.4 (16.7)
ANGLE FROM UPSTREAM, θ, DEG											
46.8	50.0	58.5	72.2	80	90.9	100	104	110	116.8	120	130.4

Figure 1. Experimental apparatus for validation case[17].

De Gennaro et al. [14] performed the only available numerical study on this test case in 2010, using ANSYS FLUENT to utilize a RANS coupled solver using a k-ω SST turbulence model on a periodic sliced domain of 10.5 million cells containing only 1 blade. Acoustic performance was simulated through a Ffowcs Williams-Hawkings Solver. Two simulations were performed: one at 0.6 Mach and one at 0.8 Mach, both corresponding to experimental measurements performed by Dittmar [16]. Note that in order to match the measured power coefficient, De Gennaro et al. increased the blade pitch angle to 60 degrees (compared to the experimental value of 59 degrees) leading to a power coefficient of 1.34 compared to the experimental value of 1.32.

B. Using Wind Tunnel Data to Validate Propeller Aeroacoustic Simulations

The conditions of a wind tunnel, governed by an interior flow, are different than typical simulations of a propeller in unbounded space or in flight. In numerical simulations, the wind tunnel is typically not modeled in order to significantly decrease computational time, resuling in a simulation of a propeller in unbounded space. Consequently, adjustments can be made to wind tunnel data to better represent acoustic conditions of flight or a numerical simulation. Dittmar and Lasagna compared flight tests to wind tunnel tests using an 8-bladed, 0.622 m diameter SR-3 propeller across flight speeds of 0.6 to 0.8 Mach[18]. Excellent comparison of results was found after adjustments made for differences in atmospheric conditions such as pressure and for differences in the distance of noise measurement locations in the same direction. These two adjustments are also seen in the numerical simulations of Whitefield [11] alongside other studies[19,20] which make similar adjustments. The adjustment for pressure shall be made for the results of the simulation according to Eq. 1:

$$SPL = SPL_{sim} - 20\, log_{10}(p_{sim}/p_{wind\ tunnel}) \tag{1}$$

where SPL is the sound pressure level, SPL_{sim} is the SPL outputted by the simulation, p_{sim} is the calculated simulation pressure, and $p_{wind\ tunnel}$ is the measured pressure in the wind tunnel. An adjustment for mic location is not necessary as the simulation mics will match those in the experiment.

Other effects can bring in discrepancy between the wind tunnel and a simulated propeller in free space. The wind tunnel, an interior flow, will generate a significant amount of broadband noise at high speeds as can be seen in experiments which present wind tunnel noise data such as that by Soderman and Horne[21] where much of the non-tonal noise is supplied by the wind tunnel noise. Nonlinear effects have been calculated in papers such as that of Hanson[22], for a propeller similar to the SR-2 propeller simulated in this work. This effect, however, is relatively small, amounting to about 1 dB for the test case studied. Both of these adjustments will be neglected in this paper as Dittmar[16] does not provide any wind tunnel data and as the magnitude of the propeller and the non-linear effects are quite small.

II. Numerical Method

All simulations were performed in STAR CCM+ using 40 Intel Xeon E7-4860 processors. The aerodynamic calcuations were governed by unsteady RANS equations with the k-ω SST model defined by Menter[23]. An implicit coupled flow scheme was used with a second-order upwind discretization scheme using Liou's AUSM+ flux vector splitting scheme[24]. Temporal discretization was calculated with a second order dual time stepping method. Gradients were computed using the Hybrid Gauss-Least Squares method for the reconstruction gradients followed by a Venkatakrishnan limiter for gradient limiting. An algebraic multigrid method was used with an implicit Gauss-Siedel relaxation scheme incorporating a Bi-Conjugate Gradient Stabilizing method. A hybrid wall function was used to resolve boundary layer flows, utilizing a wall function only for regions which did not have sufficiently small y^+ values to resolve the boundary layer without such a function.

The aeroacoustic computation was performed with the Farassat 1A Formulation[25] of the Ffowcs Williams-Hawkings equation using impermeable surfaces. This equation calculates the noise generated due to three mechanisms: 1) thickness noise generated from the displacement of air due to the geometry of the blades, 2) loading noise generated by the forces exerted on the air by the propeller, and 3) quadrupole noise, which describes noise sources away from the surface of the blade such as vortex noise. The total noise is described by the addition of the thickness, loading, and quadrupole terms. The influence of quadrupole noise is generally small for subsonic propellers. Hanson[22] showed that quadrupole noise for a similar propeller as that studied in this paper accounts for less than one dB given the tip Mach number of 0.86 in the validation case. Thus, quadrupole noise is neglected in this paper.

The thickness, p'_T, and loading terms, p'_L, of the Farassat 1A formulation are shown in Eq. 2 and Eq. 3, respectively.

$$p'_T(\boldsymbol{x},t) = \frac{1}{4\pi}\left(\int_{(f=0)} \left[\frac{\rho_0(\dot{\boldsymbol{U}}_n + \boldsymbol{U}_n)}{\boldsymbol{r}(1-\boldsymbol{M}_r)^2}\right]_{ret} d\tilde{\boldsymbol{a}} + \int_{(f=0)} \left[\frac{\rho_0 \boldsymbol{U}_n[\boldsymbol{r}\dot{\boldsymbol{M}}_r + c_0(\boldsymbol{M}_r - \boldsymbol{M}^2)]}{r^2(1-\boldsymbol{M}_r)^3}\right]_{ret} d\tilde{\boldsymbol{a}} \right) \tag{2}$$

$$\begin{aligned} p'_L(\boldsymbol{x},t) = \frac{1}{4\pi}\Bigg(& \frac{1}{c_0}\int_{(f=0)} \left[\frac{\overline{\boldsymbol{L}_r}}{\boldsymbol{r}(1-\boldsymbol{M}_r)^2}\right]_{ret} d\tilde{\boldsymbol{a}} + \int_{(f=0)} \left[\frac{\boldsymbol{L}_r - \boldsymbol{L}_M}{\boldsymbol{r}^2(1-\boldsymbol{M}_r)^3}\right]_{ret} d\tilde{\boldsymbol{a}} \\ & + \frac{1}{c_0}\int_{(f=0)} \left[\frac{\boldsymbol{L}_r[\boldsymbol{r}\overline{\boldsymbol{M}_r} + a_0(\boldsymbol{M}_r - \boldsymbol{M}^2)]}{\boldsymbol{r}^2(1-\boldsymbol{M}_r)^3}\right]_{ret} d\tilde{\boldsymbol{a}} \Bigg) \end{aligned} \tag{3}$$

where $\boldsymbol{U}_i = \left(1 - \frac{\rho}{\rho_0}\right)\boldsymbol{v}_i + \frac{\rho \boldsymbol{u}_i}{\rho_0}$, $\boldsymbol{M}_i = \frac{\boldsymbol{U}_i}{c_0}$, $\boldsymbol{L}_i = \boldsymbol{P}_{ij}\boldsymbol{n}_i + \rho \boldsymbol{u}_i(\boldsymbol{u}_n - \boldsymbol{v}_n)$, $\boldsymbol{P}_{ij} = (p - p_0)\delta_{ij} - \boldsymbol{T}_{\boldsymbol{v}_{ij}}$, $\boldsymbol{u}_i$ represents fluid velocity in the x_i direction, $\boldsymbol{u}_n$ is the fluid velocity component normal to the surface, $\boldsymbol{n}_i$ is the surface normal vector, $\boldsymbol{v}_i$ represents surface velocity in the x_i direction, $\boldsymbol{v}_n$ is the surface velocity component normal to the surface, ρ_0 and p_0 are the far field density and pressure, respectively, $\boldsymbol{r}$ is the distance from the propeller surface to the mic, and ret stands for retarded time as defined in the derivation of Farassat 1A[25]. f defines a Ffowcs Williams Hawkings surface, such that any value greater than zero is outside the surface and $f = 0$ defines the surface. A dot above a variable denotes the time derivative with respect to the source time of that variable.

III. Simulation Setup

A. Boundary Conditions and Meshing

The computational domain chosen consists of a cylinder extending a distance of 10 diameters in the radial direction, 11 diameters upstream and 21.5 diameters downstream from the propeller (Fig. 2). The propeller was constructed in PTC Creo with 21 blade elements according to the definition of the SR-2 propeller found in the experiment description[17] with 8 blades, a diameter of 0.622 m, and a root pitch angle of 60.5 degrees. An area-ruled spinner was constructed according to the geometry of the SR-2 spinner from Stefko and Jeracki [27] with a shaft which extends all the way through the domain. A stationary region enclosed a rotating cylindrical region which encapsulates the propeller, resulting in two regions for this sliding mesh simulation. The rotating cylinder has a diameter of 0.84 m (135% of the propeller diameter), extending 0.21 m upstream and 0.42 m downstream of the propeller. A view of the mesh around the propeller is shown in Fig. 3 in which the boundary of the rotating region can be seen as the thin line encapsulating the propeller which is the prism layer on the interface between the stationary and rotational regions.

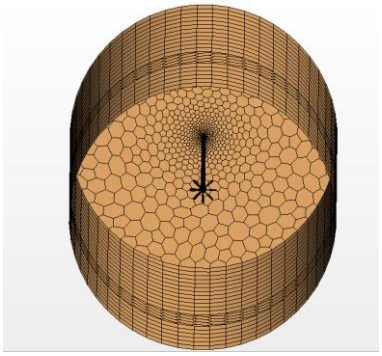

Figure 2. The computational domain around the propeller.

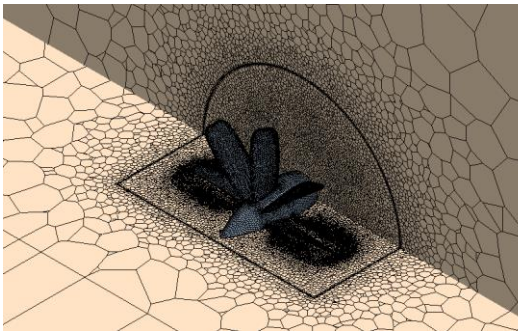

Figure 3. The mesh around the propeller.

The outer boundaries of the domain were set to the experimental freestream condition of 0.6 Mach and the propeller, spinner, and shaft were modeled as smooth no-slip walls. A polyhedral grid, consisting of 7.6 million cells was constructed with general properties outlined in Table 3. A grid was created for the domain extending 1 diameter upstream

and 1.5 diameters downstream of the propeller. This grid was then extruded orthogonally to fill out the entire domain, with 6 upstream extrusion layers and 12 downstream layers.

B. Solution Procedure

Before the unsteady simulation was performed, a steady simulation was used to initialize the flow parameters using three steps:

1) The solution was initialized with a constant velocity of 206 m/s (0.6 Mach).
2) A grid sequencing method was used with 10 grid levels and 50 iterations per level with a CFL number of 5.
3) The steady state simulation was run for 3000 iterations with a CFL number of 5.

Table 3. Mesh Properties for Validation Case

Grid Property	Value
Number of Cells	7,555,253
Prism Layer (Propeller and Spinner)	
Prism Layers	30
Prism Layer Stretch Function	Geometric Progression
Prism Layer Thickness	1 x 10^{-3} m
Thickness of Near Wall Prism Layer	1 x 10^{-7} m
Prism Layer (Stationary-Rotational Interface)	
Prism Layers	1 (in both directions)
Prism Layer Thickness	1.9 x 10^{-3} m
Prism Layer (Shaft)	
Prism Layers	2
Prism Layer Stretch Factor	1.5
Prism Layer Thickness	1 x 10^{-3} m

This process resulted in converged thrust and torque values and the resultant flow field was used to initialize the unsteady simulation.

This unsteady solution was run using a sliding mesh method for a duration of just over 5 revolutions with 720 time steps per revolution. 12 inner iterations were used per time step in the dual time-stepping process. The CFL number for the inner iterations was set to 1, and the turbulence under-relaxation factor was set to 0.5 to ensure an order of magnitude reduction in the residuals across each timestep. The only residual which did not decrease an order of magnitude across each time step was the standard turbulence dissipation rate, but even a significant variation of simulation parameters did not improve this.

It should be noted that the simulation used a root blade pitch angle of 60 degrees compared to the experimental value of 59 degrees. This pitch angle was selected in order to match the measured power coefficient (C_P) of the experiment such that the loading forces in the Ffowcs-Willaims Hawkings equation can be accurately represented. It was found that a blade pitch angle of 59 degrees only produced a C_P of 1.03, while a pitch angle of 60 degrees produced a C_P of 1.31 compared to the experimental value of 1.32. Thus, a pitch angle of 60 degrees was selected for this simulation in order to correctly capture the forces thus enabling correct aeroacoustic computation.

The power coefficient can be calculated according to Eq. 4, where P denotes power, ω denotes rotational speed, and D denotes diameter.

$$C_P = \frac{P}{\rho \omega^3 D^5} \tag{4}$$

C. Verification

Grid convergence studies were perfomed for both the aerodynamic values of thrust and torque as well as the aeroacoustic values of harmonic noise. Additionally, boundary layer thickness and refinement were compared for the base case mesh. Grids using 15-50 prism layers were tested with boundary layer thickness from 0.0005 m to 0.0015 m, resulting in the selected most efficient case of 30 prism layers with an overall thickness of 0.001 m. Converged thrust, torque, and harmonic noise values for steady state simulations were compared for meshes of 3.5, 7.6 (the base case), and 12.6 million cells with an unsteady simulation of 5 revolutions and 720 time steps per revolution. These results are summarized in Table 4, demonstrating that the thrust, torque, and harmonic noise values are all well described by the selected mesh of 7.6 million cells.

Table 4. Grid Verification Tests

Grid Size (Million Cells)	Thrust (N)	Torque (Nm)	Mic 2 Harmonics		Mic 6 Harmonics		Mic 9 Harmonics	
			First (dB)	Second (dB)	First (dB)	Second (dB)	First (dB)	Second (dB)
3.5	630	279	122.6	95.6	134.5	115.4	132.0	111.2
7.6*	615*	271*	124.0	95.9	135.8	116.9	133.2	112.4
12.6	616	270	124.0	94.5	135.8	116.7	133.2	112.3

*simulated parameters

D. Validation Results

The unsteady simulation had a wall clock time of 281 seconds per time step, taking a total of 309 wall clock hours to complete. The simulation predicted average thrust values of 615 N and average thrust values of 271 Nm, resulting

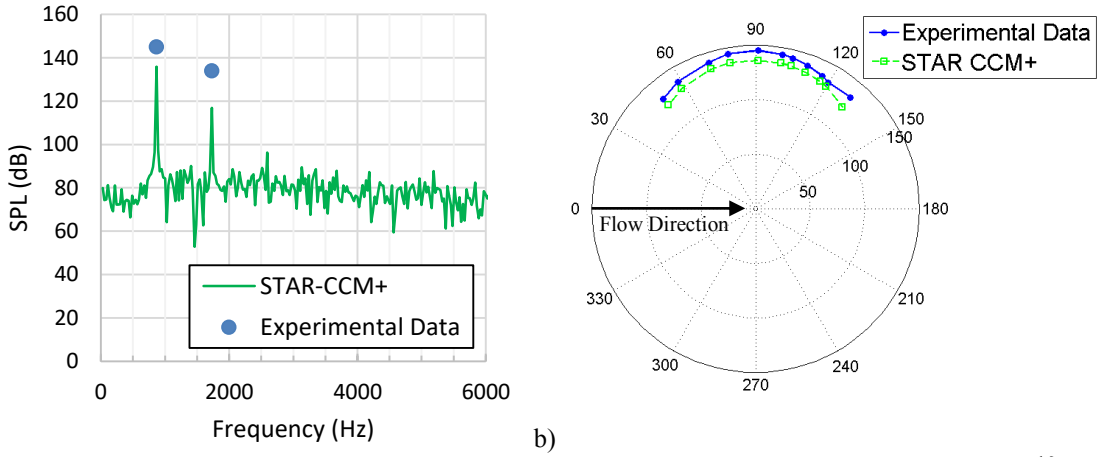

Figure 4. Simulation results, showing simulated noise from mic 6 relative to experimental values[16] (a) and directivity of first harmonic relative to experimental values[16] for all mics (b).

in a C_P of 1.31 compared to the experimental value of 1.32[16], which is the only aerodynamic data published in the experiment.

Acoustic data was computed from a single block of the last 4 revolutions of simulation, neglecting the first revolution due to the intial transient as the unsteady simulation started. An SPL plot of the loudest noise measurement, at microphone 6, is shown in Fig. 4. The first harmonic directivity relative to the experiment is also plotted in Fig.4 compared to the experiment. Harmonic levels predicted by the simulation compared to the experiment are shown in Table 5. The magnitude of the first harmonics were under-predicted by 4 to 11 dB for all mics, and the second harmonics were under-predicted more significantly, by 9 to 33 dB. The worst prediction of the second harmonics occurs at the mics furthest from the propeller plane, perhaps influenced more by the background noise of the wind tunnel than the other mics because of lower noise values for harmonics at these microphones.

These results show that the simulation can successfully reproduce propeller harmonic values particularly in the loudest regions near the propeller plane, though the absolute magnitudes of the harmonics are not fully captured. This indicates that the the propeller in the experimental condition experienced higher blade loading than that predicted by the simulation. It should be noted that the experimental conditions can be difficult to reproduce due to the lack of aerodynamic data for rigorous validation of the flow field as well as the effect of the wind tunnel on the propeller noise. These results, however, are very promising, paving the way towards feasible high-fidelity modeling of propeller aeroacoustics using a hybrid method utilizing URANS and FW-H techniques.

E. Impact of Blade Pitch Angle on Propeller Harmonic Noise

In this paper, as well as in a previous paper by De Genaro et al.[14], the blade angle of the propeller was increased by one degree from the experimental value of 59 degrees. This was done to increase the propeller loading to match the provided power coefficient value, which is defined based on the simulation torque. This was the only aerodynamic matching data available for this simulation. Adjusting the blade pitch angle assumes that the measured power coefficient is a more accurate measurement than the blade pitch angle.

In addition to the simulation performed with a blade pitch angle of 60 degrees, which had a similar power coefficient to experimental values, another simulation was performed with the experimental blade pitch angle of 59 degrees with a similar mesh and the same simulation procedure. As the results show, the variation in thrust and torque is significant, though the impact on propeller harmonic noise levels are within 1-2 dB for both the first and second harmonics across different microphones.

Table 5. Magnitudes of Simulated Blade Passage Harmonics

Mic	Harmonic Number	Frequency (Hz)	Experimental Data (dB)	Simulation Data (dB)
2	1	865	131.5	124.0
3	1	865	136.5	129.3
4	1	865	140.5	134.4
	2	1730	137.5	114.3
5	1	865	144.0	135.8
	2	1730	132.0	116.7
6	1	865	145.0	135.8
	2	1730	134.0	116.9
7	1	865	143.5	135.4
	2	1730	129.5	116.3
8	1	865	142.0	134.8
	2	1730	125.0	115.1
9	1	865	139.5	133.2
	2	1730	122.0	112.4
10	1	865	136.0	130.7
	2	1730	124.5	108.1
11	1	865	133.5	129.2
	2	1730	125.0	105.6
12	1	865	134.0	122.7
	2	1730	127.5	94.8

Table 5. Impact of Blade Pitching on Aerodynamic and Aeroacoustic Results

Grid Size (Million Cells)	Thrust (N)	Torque (Nm)	Mic 2 Harmonics		Mic 6 Harmonics		Mic 9 Harmonics	
			First (dB)	Second (dB)	First (dB)	Second (dB)	First (dB)	Second (dB)
7.6*	615*	271*	124.0	95.9	135.8	116.9	133.2	112.4
7.6	505	218	122.6	94.5	134.5	116.0	131.9	111.7

*results presented in this paper

IV. Conclusions

An unsteady RANS simulation of propeller aerodynamics coupled with the Ffowcs Williams-Hawkings equation utilizing a 7.6 million cell mesh has been completed in STAR CCM+, simulating first harmonic noise across 11 microphones within 4 to 11 dB and second harmonic noise within 9 to 32 dB. This simulation, performed on 40 processors in 13 days, shows that effective unsteady RANS simulations are feasible in a relatively small amount of time with moderate computing power. The under-prediction of harmonic levels in this paper provides a future research direction performing further simulations with refined inputs, boundary conditions, and perhaps the artificial increasing of blade loading to obtain better results.

This work shows the feasibility of using an advanced aerodynamic and aeroacoustic prediction method to simulate a complete rotating propeller domain with accurate aeroacoustic results. This has resulted in more accurate predictions of propeller noise than previously accomplished for this high speed propeller test case. The lack of aerodynamic matching data highlights the need for the publication of further benchmarking experiments for high speed propellers in order to ensure that future studies capture the flow physics as accurately as possible.

Ackowledgements

This research was completed in collaboration with Pratt & Whitney Canada and supported by the Green Aviation Research and Development Network (GARDN).

References

[1] Magliozzi, B., Hanson, D. B., and Amiet, R. K., "Propeller and Propfan Noise," *Aeroacoustics of Flight Vehicles: Theory and Practice*, 2004, pp. 1–61.

[2] Mikkelson, D. C., Mitchell, G. A., and Bober, L. J., "Summary of Recent NASA Propeller Research," *Nasa TM 83733*, 1984.

[3] Lynam, F. J. H., and Webb, H. A., "The Emission of Sound by Airscrews," *NACA TM 624*, 1919, pp. 792–801.

[4] Metzger, F. B., "An Assessment of Propeller Aircraft Noise Reduction Technology," *NASA Contractor Report*, 1995.

[5] Gutin, L., "On the Sound Field of a Rotating Propeller," *NACA TM 1195*, 1936.

[6] Lighthill, M. J., "On Sound Generated Aerodynamically -I. General Theory," *Proceedings of the Royal Society*, 1952, pp. 564–587.

[7] Ffowcs Williams, J. E., and Hawkings, D. L., "Sound Generation by Turbulence and Surfaces in Arbitrary Motion," *Philosophical Transactions of the Royal Society of London*, vol. A264, 1969, pp. 321–342.

[8] Succi, G. P., Munro, D. H., and Zimmer, J. A., "Experimental Verification of Propeller Noise Prediction," *AIAA Journal*, vol. 20, 1982, pp. 1483–1491.

[9] Schulten, J. B. H. M., "Frequency-Domain Method for the Computation of Propeller Acoustics," *AIAA Journal*, vol. 26, 1988, pp. 1027–1035.

[10] Nallasamy, M., Woodward, R. P., and Groeneweg, J. F., "High-Speed Propeller Performance and Noise Predictions at Takeoff/Landing Conditions," *Journal of Aircraft*, vol. 26, 1989, pp. 563–569.

[11] Whitefield, C. E., Gliebe, P. R., Mani, R., and Mungur, P., "High Speed Turboprop Aeroacoustic Study (Single Rotation)," *NASA CR 182257*, 1989.

[12] Schulten, J. B. H. M., "Effects of Asymmetric Inflow on Near-Field Propeller Noise," vol. 34, 1996.

[13] Schulten, J. B. H. M., "Comparison of measured and predicted noise of the Brite-EuRam SNAAP advanced propellers," *3rd AIAA/CEAS Aeroacoustics Conference*, 1997, pp. 923–933.

[14] De Gennaro, M., Caridi, D., and Pourkashanian, M., "Ffowcs Williams-Hawkings Acoustic Analogy for Simulation of Nasa SR2 Propeller Noise in Transonic Cruise Condition," *V European Conference on Computational Fluid Dynamics*, Lisbon, Portugal: 2010.

[15] Boots, D., and Feszty, D., "Numerical Investigation of the Effect of Wing Position on the Aeroacoustic Field of a Propeller," *52nd AIAA/SAE/ASEE Joint Propulsion Conference*, Salt Lake City, UT: AIAA, 2016.

[16] Dittmar, J. H., *Cruise Noise of the SR-2 Propeller Model in a Wind Tunnel*, 1989.

[17] Dittmar, J. H., *Further Comparison of Wind Tunnel and Airplane Acoustic Data for Advanced Design High Speed*, 1985.

[18] Dittmar, J. H., and Lasagna, P. L., "A preliminary comparison between the SR-3 propeller noise in flight and in a wind tunnel," 1982.

[19] Moussa, K., "Computational Modeling of Propeller Noise : NASA SR-7A Propeller," University of Waterloo, 2014.

[20] Marinus, B., "Multidisciplinary Optimization of Aircraft Propeller Blades," Centrale Lyon - University Lyon, 2011.

[21] Soderman, P. T., and Horne, W. C., "Acoustic and Aerodynamic Study of a Pusher-Propeller Aircraft Model," *NASA TP 3040*, 1990.

[22] Hanson, D. B., and Fink, M. R., "The importance of quadrupole sources in prediction of transonic tip speed propeller noise," *Journal of Sound and Vibration*, vol. 62, 1979, pp. 19–38.

[23] Menter, F. R., "Two-equation eddy-viscosity turbulence modeling for engineering applications," *AIAA Journal*, vol. 32, 1994, pp. 1598–1605.

[24] Liou, M. S., "A Sequel to AUSM: AUSM+," *Journal of Computational Physics*, vol. 129, 1996, pp. 364–382.

[25] Farassat, F., "Derivation of Formulations 1 and 1A of Farassat," *NASA TM 214852*, 2007, pp. 1–25.